Aerosol assisted atmospheric pressure plasma jet for a high deposition rate of silica-like thin films

Romain Magnan, Richard Clergereaux, Christina Villeneuve-Faure, Benoît Lantin, Guillaume Carnide, Patrice Raynaud, Nicolas Naude

Aerosol assisted atmospheric pressure plasma jet for a high deposition rate of silica-like thin films

Romain MAGNAN[1], Richard CLERGEREAUX[1], Christina VILLENEUVE-FAURE[1], Benoît LANTIN[1], Guillaume CARNIDE[1,2], Patrice RAYNAUD[1] and Nicolas NAUDE[1*]

[1]LAPLACE, CNRS, UPS, INPT, Université de Toulouse, Toulouse, France

[2]LCC, CNRS, Université de Toulouse, Toulouse, France

** corresponding author: nicolas.naude@laplace.univ-tlse.fr*

ABSTRACT

This paper investigated thin films deposition processes of silica-like based on the injection of liquid droplets in Atmospheric Pressure Plasma Jet – APPJ operated in open air at atmospheric pressure. An aerosol of hexamethyldisilane is produced by a syringe-pump and injected in a nitrogen post-discharge for different liquid precursor and carrier gas flow rates. For high carrier gas flow, this process enables to form silica-like without addition of oxygen in the plasma phase. This process offers a thin film dynamic deposition rate from 500 to 1400 nm.m.min^{-1} depending on the carrier gas flow and the film structure departs from silica-like to organosilicon layers for the lowest flow rates. These evolutions are attributed to plasma - droplets interactions related to the transport of droplets, the evaporation of liquid and plasma polymerization.

Keywords: aerosol-assisted process, plasma deposition, thin film coating, hexamethyldisilane, non-equilibrium plasma, atmospheric pressure

1. INTRODUCTION

Plasma enhanced chemical vapor deposition (PECVD) enables to form a wide range of materials in thin films. Those deposited from silicon-based precursors develop different properties such as barrier coating, transparency and insulating properties relevant for various applications like packaging [1], [2], anticorrosion [3], [4], microelectronics [5], [6], etc. These precursors are generally injected as gases that dissociate and ionize in the plasma phase.

In recent years, atmospheric pressure plasmas have been widely studied. For example, dielectric barrier discharges (DBDs) allow to elaborate dense and homogenous thin films for large surface in-line production [7], the thin film growth rate being controlled by several process parameters such as the discharge power, the gas composition, etc. Indeed, the first parameter proportional to the excitation frequency leads to an increase of the reactive species densities and, consequently, of the growth rate. For example, in Ar-NH_3-SiH_4 mixtures, Bazinette *et al*. showed that tuning the excitation frequency from kHz to MHz leads to an increase of the growth rate from 10 up to 80 nm.min^{-1} [8]. Another set of parameters deals with the precursor, *i.e.* type, residence time and concentration. For example, the quantity of precursor injected in the gas phase can increase the deposition rate. However, it can also lead to the formation of powders in the gas phase due to an increase of the residence time [8]. To avoid such mechanisms, a lot of organosilicon precursors have been used. For example, Fanelli et *al.* showed that hexamethyldisiloxane (HMDSO) [$(CH_3)_3SiOSi(CH_3)_3$] can form various organosilicon ($SiO_xC_yH_z$) as well as silica-like (SiO_x) thin films in DBDs with deposition rates up to 100 nm.min^{-1} without powdering [9]. For silica layers, it needs adding oxygen in the gas phase. For example, FTIR spectra highlight the formation of quasi-pure SiO_2 for an O_2 / HMDSO concentration ratio larger than 25

However, DBDs are mainly adapted to processes over flat and insulating substrates [10]. Indeed, the presence of conductive materials on the electrodes is modifying the regime of

discharge and the interelectrode distance in the mm range is not easily compatible with the treatment of 3D objects. Plasma afterglows (or post-discharges) appear as more suitable methods for thin film deposition on more complex substrates. A lot of atmospheric pressure configurations, such as micro plasma jet [11] or jet [12] [13], have been developed. As an example, injection of HMDSO in Atmospheric Pressure Plasma Jet (APPJ) system working at 13.56 MHz in Ar enables to form various $SiO_xC_yH_z$ films with deposition rates in the 150 $nm.s^{-1}$ range [11], [14] without dust particles production. In addition, mounted on 3D-axis robot, it enables to coat really large surfaces, the dynamic deposition rate being directly related with the displacement velocities. However, a lot of those atmospheric plasma jets are working with noble gases [15], [16]. They are then restricted by operating costs especially due to the consumption of the carrier gas. Noble gas substitution is then crucial, for example, by nitrogen or air [17].

In addition, those deposition processes are generally using volatile and stable precursors. Indeed, to ensure an efficient injection and deposition process, the molecules should have a vapor pressure of several Pa at room temperature or at temperatures below its decomposition temperature, limiting the range of possibilities. An alternative solution deals with aerosol-assisted processes. Indeed, aerosols can be formed from liquid precursors or solutions (liquid mixtures, colloidal solutions, etc.) whatever their thermodynamic properties with an accurate flow control [15]. Coupled to APPJ, it leads to an original process at reduced cost. For example, Lommatzsch *et al.* [12] or Asadollahi *et al.* [18] deposited organosilicon thin films by injecting HMDSO as an aerosol in an APPJ. Commercially, the UL-Scan® plasma device from AcXys Plasma Technologies© has been developed to coat large surfaces. For example, Hamze *et al.* [13] used hexamethyldisilane (HMDS, $[(CH_3)_3SiSi(CH_3)_3]$) in this device: with a liquid precursor flow rate of 220 $\mu L.min^{-1}$ (9.5 $g.h^{-1}$), various $SiO_xC_yH_z$ ($y = 4 - x$ and $3 \leq x \leq 4$) films with a small roughness (around 4 nm) and low concentration of carbon are formed at dynamic

deposition rate higher than 480 nm.m.min^{-1} without addition of O_2. Indeed, post-discharge interactions with ambient air play a crucial role in thin film deposition [19]. For example, an efficient diffusion of species from the ambient air has been numerically evidenced by Reuter *et al.*[20] and measured by Dunnbier *et al.* [21]. Indeed, the latter highlighted, by optical emission spectroscopy measurements, the presence of OH* and O* formed through the decomposition of the O_2 and H_2O contaminant from ambient air along the APPJ. Because of the gas flow velocity at the APPJ output, a key role of the turbulence air incorporated in the plasma has been reported [19]. Hence, AAPJ in open air enable to deposit silica-like materials without addition of O_2. Coupled with an aerosol, these processes offer a generic process with high mass transport and thus higher deposition rates.

Our study aims to emphasize the role of plasma – droplets interactions on the deposition of silica-like coatings in the APPJ from AcXys Plasma Technologies©. The discharge, ignited in pure nitrogen, is coupled to an aerosol of HMDS produced, here, by a nebulizer and injected in the post-discharge. We focused on the role of gas and liquid flows in this aerosol-assisted process. Indeed, silica-like is obtained for high carrier gas flow rates. This process is controlled by different mechanisms of interaction between the aerosol (controlled by the liquid and gas flow rates) and the post-discharge, namely, the transport of droplets, the evaporation of the liquid and the precursor plasma polymerization.

2.EXPERIMENTAL DETAILS

The liquid injection and the plasma systems used in this work are schematically described in **Figure 1**.

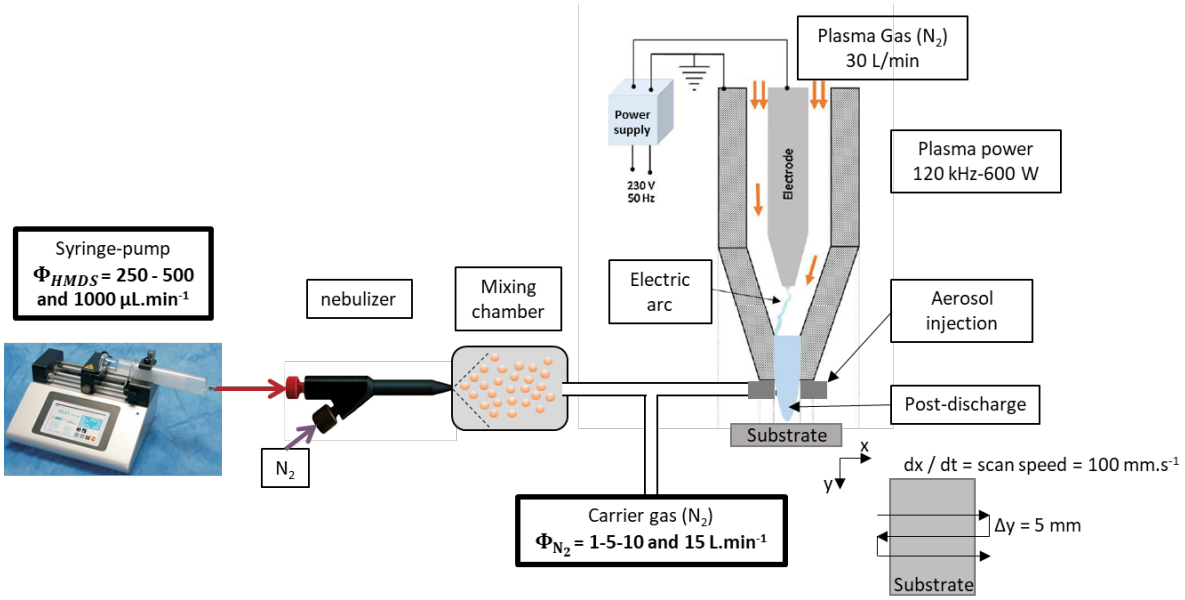

Figure 1. Details of the APPJ coupled with the injection system modified/updated from [22].

The plasma process consisted in an industrial arc plasma torch UL-SCAN supplied by AcXys Technologies©. It consists in a transferred arc used to produce an Atmospheric Pressure Plasma Jet – APPJ. The arc was ignited at an excitation frequency fixed at 120 kHz corresponding to a discharge power of 600 W. It was formed in pure N_2 injected at 30 L.min^{-1} and the post-discharge operated in open air. The distance between the substrate and the nozzle was set at 1 cm and APPJ interacting surface with the substrate is a circular spot of 5 mm diameter.

HMDS (purity >98% from Thermo Fisher Scientific©) was injected as an aerosol in the post-discharge, *i.e.* at the exhaust of the nozzle as presented in **Figure 1**. It was transported from a syringe pump with a flow rate (Φ_{HMDS}) set between 250 and 1000 µL.min^{-1} (corresponding to 10.7 – 42.9 g.h^{-1}) to a pneumatic nebulizer (Mira Mist from Burgener research supplied with N_2 flow equal to 0.9 L.min^{-1}) that generated the aerosol of liquid droplets.

At the exit of the nebulizer, it was diluted in a mixing chamber with a carrier gas (N_2) set at a flow rate (Φ_{N_2}) ranging from 1 and 15 L.min^{-1} and transported toward the post-discharge through a nozzle with four holes.

To form 2D coatings, the APPJ was mounted on a 3-axis robot. With a scan speed (along x-axis) set at $v_S = 6$ m.min^{-1} (100 mm.s^{-1}) and a displacement along the y-axis (Δy) at 5 mm (**Figure 1**). In these conditions, one pass on a surface of 10×10 cm^2 lasted around 20 s.

Before coating, the intrinsic silicon substrate was pre-treated by one plasma passing without liquid precursor. Thin films were then deposited for different HMDS (Φ_{HMDS}) and N_2 carrier gas (Φ_{N_2}) flow rates using the parameters summarized in **table 1**. For the deposition process, the number of APPJ passes is arbitrary set to N=3.

Table 1. Experiment parameters summary

		Pre-treatment	**Deposition**
Plasma	Gas	N_2	N_2
	Flow rate (L.min^{-1})	30	30
	Frequency (kHz)	120	120
	Power (W)	600	600
	APPJ passes	1	3
Precursor	Liquid	-	HMDS
	Flow rate (µL.min^{-1})	-	250/500/1000
Carrier gas	Gas	-	N_2
	Flow rate (L.min^{-1})	-	1/5/10/15

The film thickness, d, was determined by profilometry using a TENCOR alpha step IQ. In order to compare our result to ones reported by Lommatzsch *et al* [12] or Hamze *et al* [13], the

dynamic thin film growth rate, v (in $nm.m.min^{-1}$), was determined from the film thickness (d), considering the number of pass (N) and the scanning speed (v_S) using the equation $v = (d/N).v_S$. The surface morphology was probed by Atomic Force Microscopy (AFM BRUKER Multimode 8) in tapping mode. The root mean square roughness Rq was determined over the 5 µm x 5 µm probed surface. Images were treated using Imagej® software. The surface morphology of thin film is investigated by scanning electron microscopy (SEM FEG JEOL JSM 6700F). The image is acquired with an extraction voltage of 10 kV and a magnification of x10k.

Ellipsometric spectra recorded on a SEMILAB SE-2000 were used to define the conditions of flow rates to obtain a SiO_2 coating. The fit regression was limited to a single layer of smooth and homogeneous silica considering an Effective Medium Approximation (EMA) model of SiO_2 with void and the thickness d measured by profilometry. To emphasize the silica-like structure of the films, the accuracy of fit (R^2) was determined for the different conditions. A $R^2 > 0.9$ means a quasi-pure SiO_2 layer while a lower R^2 suggests that the coating structure departs from silica.

As a complement, Fourier Transform Infra-Red (FTIR) spectroscopy was performed by a BRUKER Vertex 70 spectrometer in transmission mode, all spectra were acquired by averaging 20 scans with a spectral resolution of 4 cm^{-1} in the range of 400-4000 cm^{-1}.

3.RESULTS AND DISCUSSION

3.1. Silica-like coatings

Silica-like thin films are obtained with the carrier gas set to Φ_{N_2} = 15 L.min^{-1} coupled with HMDS injection fixed at Φ_{HMDS} = 500 µL.min^{-1}. Indeed, ellipsometry highlights that the layer consists in SiO_2 (volume fraction of 92%) with an accuracy better than 0.95. The silica-like structure is also confirmed by FTIR as presented in **Figure 2a**. Indeed, the spectrum highlights the main features of SiO_2, *i.e.* the characteristic absorption bands of Si-O-Si located at 800 (bending), 1075 (AS1) and 1150 cm^{-1} (AS2) (asymmetric stretching) [23]. Si-OH at 923 cm^{-1} and OH between 3100 and 3800 cm^{-1} related to hydroxyl groups as well as Si-$(CH_3)_x$ bending absorption at 1270 cm^{-1} and CH_x stretching mode at 2960 cm^{-1} are also observed in small abundance. These bands are characteristics of the incomplete fragmentation of the organosilicon precursor as classically observed in plasma deposited silica. Hence, silica-like coatings are obtained without addition of O_2. As previously reported by Asad et al. [19], due to the flow turbulence, O_2 and H_2O from ambient air can be incorporate in the post-discharge, and contribute to the plasma process (dissociation, oxidation). After 3 passes, the film thickness is found around 250 nm. Considering the scan speed and the number of pass, it corresponds to a dynamic deposition rate of about 500 nm.m.min^{-1} per pass, similar to the ones reported by Lommatzsch *et al* [12] or Hamze *et al* [13]. On a surface of 10×10 cm^2, one can estimate the deposition rate of 0.4 g.h^{-1} for an injection of 21 g.h^{-1} of HMDS.

Finally, with a so high deposition rate, one can expect a high roughness. The typical AFM image presented in **Figure 2b** shows an upper roughness value of 36 nm which is in the same range as [13]. In addition, AFM as well as SEM images show the presence of spheres with a diameter of up to 500 nm. Such spheres suggest a contribution of liquid droplets in the deposition process. Considering an initial droplet size of few µm at the exhaust of the nebulizer

[13], [24], it suggests that a lot of plasma – droplet interactions are involved, as plasma polymerization and/or thermal evaporation of the liquid.

a) b)

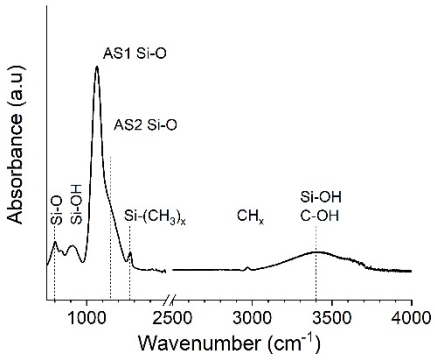

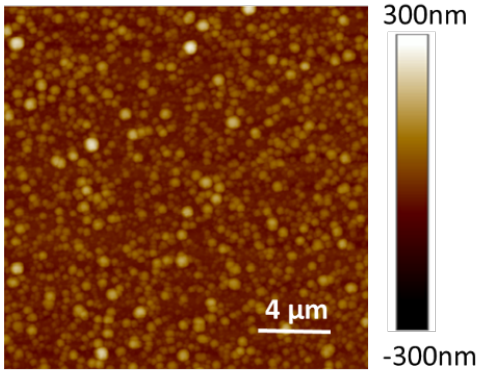

c)

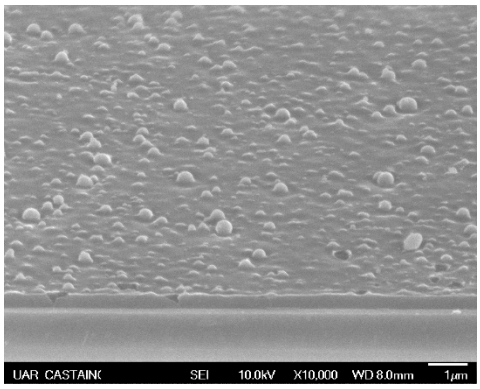

Figure 2. Thin film deposited for $\boldsymbol{\Phi_{HMDS}}$ = 500 µL.min^{-1} and $\boldsymbol{\Phi_{N_2}}$ = 15 L.min^{-1} **a)** AFM image and **b)** FTIR spectra and **c)** SEM image of the surface

Hence, this process is forming silica-like coatings at high deposition rate. One can rely these observations to the aerosol. In order to further investigate the plasma – droplet interactions, the effects of the precursor and carrier gas flow rates are discussed in the following parts.

3.2. Influence of the liquid precursor flow rate

Thin films were deposited for different precursor flow rate Φ_{HMDS}, whereas Φ_{N_2} being unchanged and set to 15 L.min^{-1}. As presented in **Figures 3a**, the thicknesses and roughnesses are slightly affected by Φ_{HMDS}. Whatever the precursor flow rate, the thin film thickness is ranging between 250 and 300 nm – corresponding to a dynamic deposition rate of about 500-600 nm.m.min^{-1}. The plasma deposition rate seems to be limited by the conversion efficiency related to the low plasma power injected in these experiments. In addition, the roughness remains constant around 35 nm and the surface morphology highlights the presence of the same spherical shape with a size around 500 nm evenly distributed whatever the precursor flow rate (**Figures 3d-c-d**).

a)

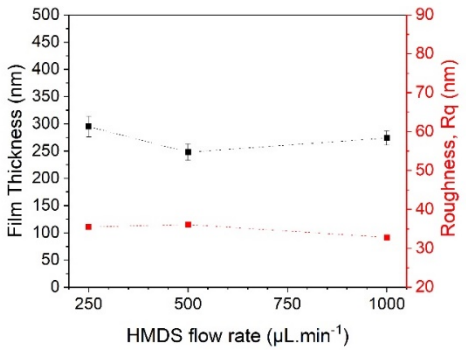

b) c) d)

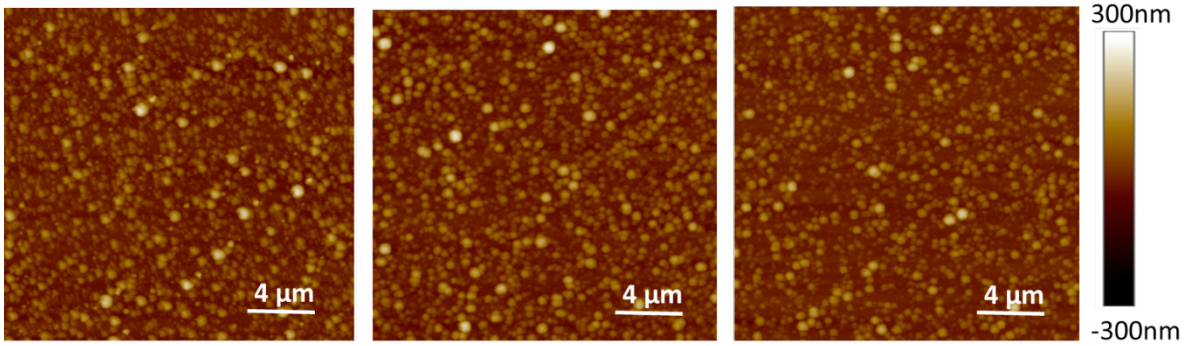

Figure 3. a) Evolution of the thin film thickness d and Rq as a function of the precursor flow rate for Φ_{N_2} = 15 L.min^{-1}. 5 µm x 5 µm AFM surface topography mapping for Φ_{N_2} = 15 L.min^{-1} and **b)** Φ_{HMDS} = 250 µL.min^{-1} **c)** Φ_{HMDS} = 500 µL.min^{-1} and **d)** Φ_{HMDS} = 1000 µL.min^{-1}.

To emphasize the effect of Φ_{HMDS} on the aerosol, rapid images of the light (green LED at λ= 530 nm) scattered by the aerosol at the exhaust of the nebulizer are recorded by a CCD camera for different conditions. **Figure 4a** shows typical pictures taken for various Φ_{HMDS}: it highlights that the aerosol consists in a dense fog, the scattered light intensity increasing with the flow rate, *i.e.* with the quantity of liquid injected in the aerosol. The scattered light integrated on the whole picture is reported as a function of the flow rate in **Figure 4b**. Considering Mie-scattering, the linear variation of the scattered light intensity with Φ_{HMDS} cannot be attributed to the droplets size – the latter remaining constant for the same liquid at a fixed temperature and pressure [25]. It suggests that Φ_{HMDS} is only increasing the number of droplets injected in the post-discharge.

a)

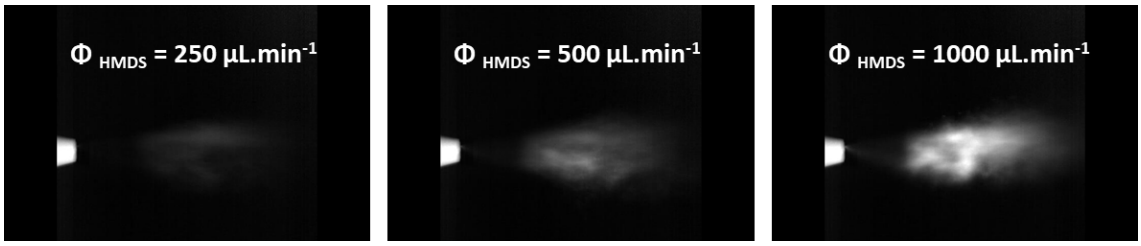

b)

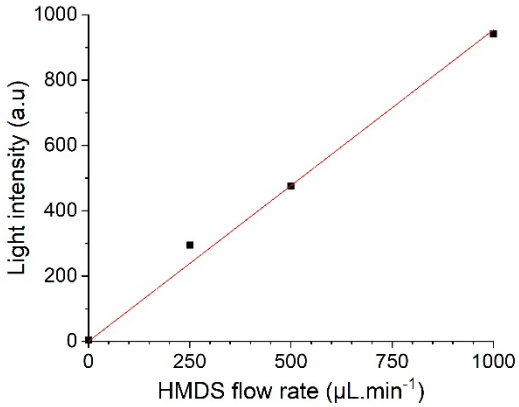

Figure 4. a) Photos of the aerosol at the nebulizer exit for $\boldsymbol{\Phi_{HMDS}}$ = 250, 500 and 1000 µL.min^{-1} **b)** Intensity of the light scattering as a function of the precursor flow rate (values extracted from aerosol photos).

As an increase of the precursor flow rate, *i.e.* the number of droplets, does not modify the deposition rate, it means that the deposition yield decreases. Moreover, the morphology remains unchanged.

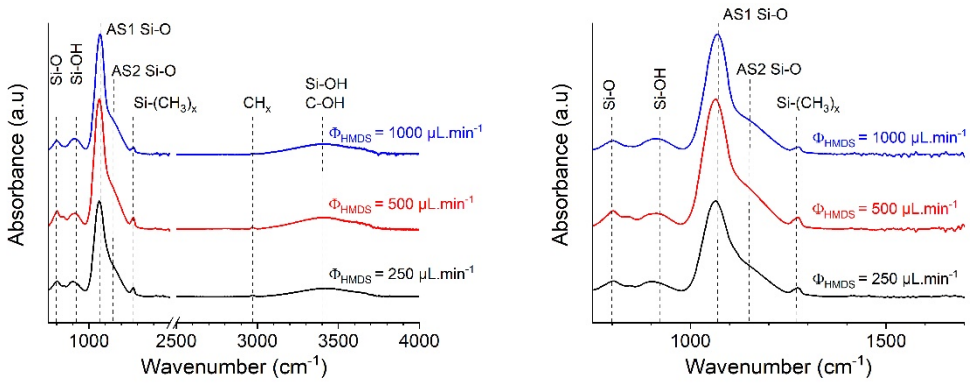

Figure 5. FTIR spectra of the thin films deposited for $\boldsymbol{\Phi_{HMDS}}$ = 250, 500 and 1000 µL.min^{-1} and $\boldsymbol{\Phi_{N_2}}$ = 15 L.min^{-1}.

Finally, FTIR shows that the film structure is also independent on the liquid flow rate Φ_{HMDS}. Indeed, the similar FTIR signature with the presence of Si-O-Si (AS1 and AS2) with a small quantity of Si-OH, Si-CH_3 and CH_x bands shows a silica-like structure of the different coatings, *i.e.* that the plasma process is not affected by the liquid flow rate.

It suggests that the deposition process is limited by plasma – droplet interactions. In these conditions, we assume that the plasma power limits the conversion/decomposition of the precursor. With the range of HMDS flow rate studied here, these interactions are saturated leading to a process mass balance decreasing with Φ_{HMDS}.

3.3. Influence of carrier gas flow rate

To study and highlight the effects of transport, the role of the carrier gas is studied and the precursor flow rate, Φ_{HMDS}, being set at 500 µL.min^{-1}. **Figure 6** reports the evolution of the film thickness, surface roughness and surface morphology from the previous optimal condition, Φ_{N_2} = 15 L.min^{-1} down to 1 L.min^{-1}.

Both, the film thickness and the roughness, are decreasing with the carrier gas flow rate suggesting that plasma – droplets interactions are modified (**Figure 6**). For example, it can affect the transport of droplets: the lower the carrier gas flow rate, the lower the driving of the aerosol with the carrier gas. Hence, the thickness would be lowered for small Φ_{N_2}.

However, AFM shows that the surface morphology is also affected by the carrier gas flow rate (**Figure 6b-c-d)**. From about 500 nm observed for Φ_{N_2} = 15 L.min^{-1}, the size of the spherical grains observed on the sample are more abundant and larger, around 700 nm, for Φ_{N_2} = 1 L.min^{-1}. It implies that the form of the aerosol is also modified by the gas flow rate. Hence, the role of droplet transport is not so direct. On one hand, the carrier gas flow rate can efficiently transport the aerosol to the center of the post discharge, thus improving the dissociation and plasma polymerization of the precursor, as droplets of liquid. On the other hand, at higher N_2 flow rate, evaporation of the liquid in the aerosol can increase, improving the dissociation of the precursor, as a gas, in the post discharge. The latter case would densify the film as observed experimentally from the variations of the roughness.

Hence, with the variation of the thickness and, consequently, the deposition rate, the carrier gas flow rate must increase the deposition yield.

a)

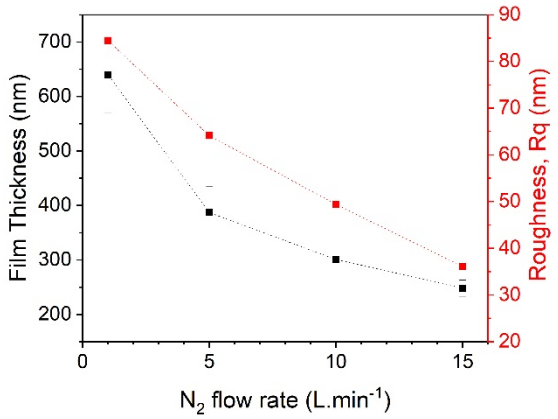

b) c) d)

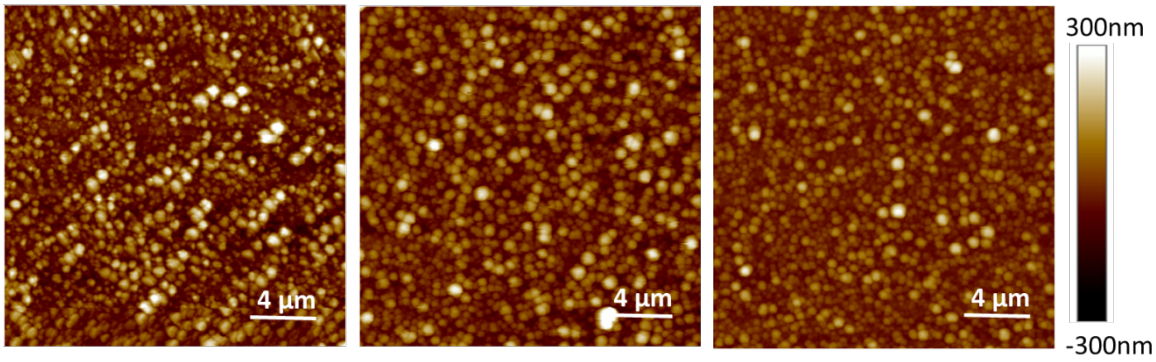

Figure 6. a) Evolution of the thin film thickness and roughness as a function of the carrier gas flow rate for Φ_{HMDS} = 500 µL.min^{-1}. 5 µm x 5 µm AFM surface topography mapping for Φ_{HMDS} = 500 µL.min^{-1} and **b)** Φ_{N_2} = 1 L.min^{-1}, **c)** Φ_{N_2} = 5 L.min^{-1} and **d)** Φ_{N_2} = 10 L.min^{-1}.

This is true if the film structure is independent on the carrier gas flow. However, drastic modifications are observed on the FTIR spectra (**Figure 7a**). Especially, in the 1000 to 1200 cm^{-1} range (inset **Figure 7a**), though FTIR spectra are dominated by a large band corresponding to the asymmetric stretching modes of Si-O-Si with a maximum at 1073 cm^{-1} (AS1 mode) and a shoulder at 1200 cm^{-1} (AS2 mode), the coating obtained for different carrier gas flow rate clearly emphasize the shoulder at 1200 cm^{-1} attributed to AS2 mode. In addition, the intensity of the main band (1073 cm^{-1}) increases with the carrier gas flow rate in agreement with the intensity of the Si-CH_3 band at 1270 cm^{-1}. The latter is emphasized by the evolution of AS_1/Si-

CH_3 ratio with the flow rate (**Figure 7b**). Hence, the film at lower N_2 flow rate is more organic than the silica-like coating deposited at 15 L.min^{-1}. It means that the film density is lower, decreasing the deposition yield though the deposition rate increases.

a)

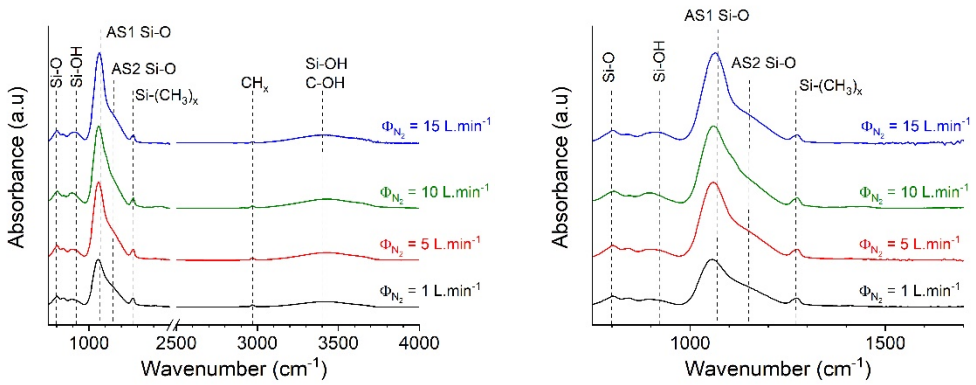

b)

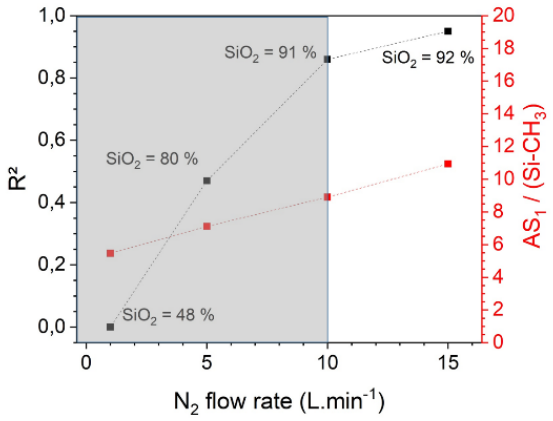

Figure 7. a) FTIR spectra of the thin films deposited for $\boldsymbol{\Phi_{N_2}}$ = 1, 5, 10 and 15 L.min^{-1} and $\boldsymbol{\Phi_{HMDS}}$ = 500 µL.min^{-1} **b)** Evolution of the ellipsometry fit precision (R^2) -from the fit regression considers a smooth and homogeneous silica-like layer, i.e. a single layer defined as a mixture of SiO_2 with void considering an Effective Medium Approximation (EMA) model- and AS_1 / $SiCH_3$ ratio as a function of the carrier gas flow rate for $\boldsymbol{\Phi_{HMDS}}$ = 500 µL.min^{-1}.

These chemical evolutions are confirmed by spectroscopic ellipsometry: silica-like structure is completely unsuitable to fit ellipsometric data of the films produced at carrier gas flow rate lower than 10 L.min^{-1} as suggested by the drastic evolution of R^2 (and the darkened area for $R^2 < 0.9$) (**Figure 7b**).

Hence, increasing the carrier gas flow rate induces a higher precursor dissociation and polymerization as well as a higher oxidation due to penetration of the droplets at the center of the plasma post discharge. However, the evaporation of the droplet can be also modified during the transport or at the center of the plasma post discharge.

As summarized in **Figure 8**, in our process conditions, the carrier gas flow rate, Φ_{N_2}, is the key parameter to control the plasma process. It is responsible of the transport of droplets in the post-discharge leading to an efficient dissociation and plasma polymerization of the organosilicon precursor. This transport can also affect the size of the droplets due to the evaporation of the liquid. The carrier gas flow enables to tailor the thin film morphology and composition whereas the liquid flow rate only increases the number of droplets in the aerosol.

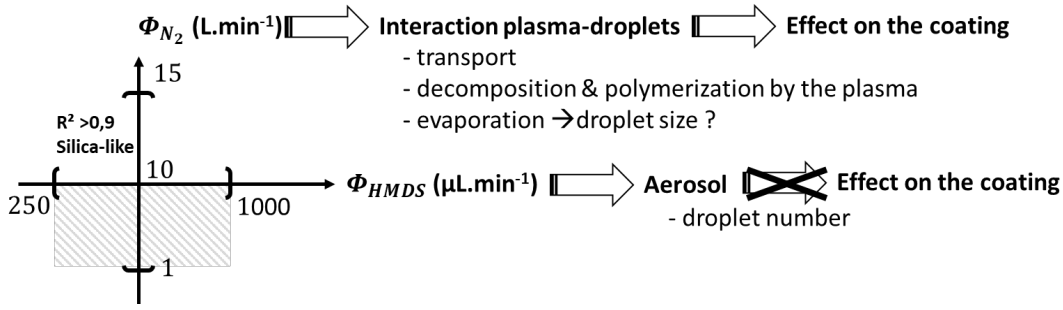

Figure 8. Roles of the carrier gas and the liquid flow rates on the aerosol-assisted APPJ process.

4.CONCLUSION

This study aimed to discuss aerosol-assisted APPJ processes. It highlights the significant effect of the aerosol on the thin film characteristics deposited. Especially, the aerosol injection parameters such as the carrier gas (N_2) and the liquid precursor (HMDS) flow rates are controlling the deposition.

While the liquid precursor flow rate does not modify the global process (deposition rate, roughness and film structure) though the number of droplets injected in the aerosol increases, pure silica is obtained at high deposition rate (500 $nm.m.min^{-1}$) if the carrier gas flow rate is high enough. It suggests that the carrier gas is transporting the droplets in the post-discharge leading to an efficient plasma polymerization and oxidation during the process. Indeed, when reducing the carrier gas flow rate, the thin films departs from pure silica to more organic and less dense coatings ($SiO_xC_yH_z$). This is attributed to a smaller penetration of the droplets inside the post-discharge related to the smaller carrier gas flow.

Deposition processes with aerosol-assisted APPJ are controlled by the plasma - droplets interactions. The latter can affect the dissociation and plasma polymerization of the precursor and the transport of the aerosol to the center of the post-discharge where it can efficiently oxidize and/or the droplet evaporation during the transport which can modify the droplet size and thus plasma - droplets interactions.

Acknowledgments

This work was supported by “region Occitanie” in France.

REFERENCE

[1] M. Creatore, F. Palumbo, R. D'Agostino, and P. Fayet, "RF plasma deposition of SiO2-like films: Plasma phase diagnostics and gas barrier film properties optimisation," *Surf. Coatings Technol.*, vol. 142–144, pp. 163–168, 2001, doi: 10.1016/S0257-8972(01)01095-7.

[2] M. Creatore, F. Palumbo, and R. D'Gostino, "Deposition of SiOx Films from Hexamethyldisiloxane/Oxygen Radiofrequency Glow Discharges: Process Optimization by Plasma Diagnostics," *Plasmas Polym.*, vol. 7, no. 3, pp. 291–310, 2002, doi: 10.1023/A:1019942625607.

[3] L. Zajíčková *et al.*, "Plasma modification of polycarbonates," *Surf. Coatings Technol.*, vol. 142–144, pp. 449–454, 2001, doi: 10.1016/S0257-8972(01)01134-3.

[4] J. Bour *et al.*, "Different ways to plasma-polymerize HMDSO in DBD configuration at atmospheric pressure for corrosion protection," *Plasma Process. Polym.*, vol. 5, no. 8, pp. 788–796, 2008, doi: 10.1002/ppap.200800052.

[5] A. Grill, "Plasma enhanced chemical vapor deposited SiCOH dielectrics: From low-k to extreme low-k interconnect materials," *J. Appl. Phys.*, vol. 93, no. 3, pp. 1785–1790, 2003, doi: 10.1063/1.1534628.

[6] A. Milella, F. Palumbo, J. L. Delattre, F. Fracassi, and R. d'Agostino, "Deposition and characterization of dielectric thin films from allyltrimethylsilane glow discharges," *Plasma Process. Polym.*, vol. 4, no. 4, pp. 425–432, 2007, doi: 10.1002/ppap.200600186.

[7] F. Massines, C. Sarra-Bournet, F. Fanelli, N. Naudé, and N. Gherardi, "Atmospheric pressure low temperature direct plasma technology: Status and challenges for thin film deposition," *Plasma Process. Polym.*, vol. 9, no. 11–12, pp. 1041–1073, 2012, doi: 10.1002/ppap.201200029.

[8] R. Bazinette, J. F. Lelièvre, L. Gaudy, and F. Massines, "Influence of the Discharge

Mode on the Optical and Passivation Properties of SiNx:H Deposited by PECVD at Atmospheric Pressure," *Energy Procedia*, vol. 92, pp. 309–316, 2016, doi: 10.1016/j.egypro.2016.07.087.

[9] F. Fanelli, S. Lovascio, R. D'Agostino, F. Arefi-Khonsari, and F. Fracassi, "Ar/HMDSO/O2 fed atmospheric pressure DBDs: Thin film deposition and GC-MS investigation of by-products," *Plasma Process. Polym.*, vol. 7, no. 7, pp. 535–543, 2010, doi: 10.1002/ppap.200900159.

[10] J. F. Lelièvre *et al.*, "Efficient silicon nitride SiNx:H antireflective and passivation layers deposited by atmospheric pressure PECVD for silicon solar cells," *Prog. Photovoltaics Res. Appl.*, vol. 27, no. 11, pp. 1007–1019, 2019, doi: 10.1002/pip.3141.

[11] V. Raballand, J. Benedikt, S. Hoffmann, M. Zimmermann, and A. Von Keudell, "Deposition of silicon dioxide films using an atmospheric pressure microplasma jet," *J. Appl. Phys.*, vol. 105, no. 8, 2009, doi: 10.1063/1.3108541.

[12] U. Lommatzsch and J. Ihde, "Plasma polymerization of HMDSO with an atmospheric pressure plasma jet for corrosion protection of aluminum and low-adhesion surfaces," *Plasma Process. Polym.*, vol. 6, no. 10, pp. 642–648, 2009, doi: 10.1002/ppap.200900032.

[13] H. Hamze, M. Jimenez, D. Deresmes, A. Beaurain, N. Nuns, and M. Traisnel, "Influence of processing gases on the properties of cold atmospheric plasma SiO x C y coatings," *Appl. Surf. Sci.*, vol. 315, no. 1, pp. 531–537, 2014, doi: 10.1016/j.apsusc.2013.12.108.

[14] H. Kakiuchi, K. Higashida, T. Shibata, H. Ohmi, T. Yamada, and K. Yasutake, "High-rate HMDSO-based coatings in open air using atmospheric-pressure plasma jet," *J. Non. Cryst. Solids*, vol. 358, no. 17, pp. 2462–2465, 2012, doi: 10.1016/j.jnoncrysol.2011.12.081.

[15] W. C. Zhu, Q. Li, X. M. Zhu, and Y. K. Pu, "Characteristics of atmospheric pressure

plasma jets emerging into ambient air and helium," *J. Phys. D. Appl. Phys.*, vol. 42, no. 20, pp. 0–4, 2009, doi: 10.1088/0022-3727/42/20/202002.

[16] A. Van Deynse, P. Cools, C. Leys, R. Morent, and N. De Geyter, "Surface modification of polyethylene in an argon atmospheric pressure plasma jet," *Surf. Coatings Technol.*, vol. 276, pp. 384–390, 2015, doi: 10.1016/j.surfcoat.2015.06.041.

[17] U. Lommatzsch, D. Pasedag, A. Baalmann, G. Ellinghorst, and H. E. Wagner, "Atmospheric pressure plasma jet treatment of polyethylene surfaces for adhesion improvement," *Plasma Process. Polym.*, vol. 4, no. SUPPL.1, pp. 1041–1045, 2007, doi: 10.1002/ppap.200732402.

[18] S. Asadollahi, J. Profili, M. Farzaneh, and L. Stafford, "Development of Organosilicon-based superhydrophobic coatings through atmospheric pressure plasma polymerization of HMDSO in nitrogen plasma," *Materials (Basel).*, vol. 12, no. 2, 2019, doi: 10.3390/ma12020219.

[19] S. S. Asad *et al.*, "Deposition of thin SiOx films by direct precursor injection in atmospheric pressure microwave torch (TIA)," *Plasma Process. Polym.*, vol. 6, no. SUPPL. 1, pp. 508–513, 2009, doi: 10.1002/ppap.200931104.

[20] S. Reuter *et al.*, "Atomic oxygen in a cold argon plasma jet: TALIF spectroscopy in ambient air with modelling and measurements of ambient species diffusion," *Plasma Sources Sci. Technol.*, vol. 21, no. 2, 2012, doi: 10.1088/0963-0252/21/2/024005.

[21] M. Dünnbier *et al.*, "Ambient air particle transport into the effluent of a cold atmospheric-pressure argon plasma jet investigated by molecular beam mass spectrometry," *J. Phys. D. Appl. Phys.*, vol. 46, no. 43, 2013, doi: 10.1088/0022-3727/46/43/435203.

[22] L. Brès, A. Sanchot, B. Rives, N. Gherardi, N. Naudé, and M. Aufray, "Fine-tuning of chemical and physical polymer surface modifications by atmospheric pressure post-

discharge plasma and its correlation with adhesion improvement," *Surf. Coatings Technol.*, vol. 362, no. January, pp. 388–396, 2019, doi: 10.1016/j.surfcoat.2019.01.102.

[23] P. G. Pai, S. S. Chao, Y. Takagi, and G. Lucovsky, " Infrared spectroscopic study of SiO x films produced by plasma enhanced chemical vapor deposition ," *J. Vac. Sci. Technol. A Vacuum, Surfaces, Film.*, vol. 4, no. 3, pp. 689–694, 1986, doi: 10.1116/1.573833.

[24] P. Fabio, "recent advancements in the use of aerosol-assisted atmospheric pressure plasma deposition," *Coatings*, 2020, doi: 10.3390/ma13132931.

[25] S. K. Friedlander, "DYNAMICS OF AEROSOL FORMATION BY CHEMICAL REACTION," *Ann. New York Acad. Sci.*, 1983.